

Nanosecond Pulsed Laser-Heated Nanocrystals Inside a Metal-Organic Framework Matrix

Max Niemeyer,^[a, c] Patrick Bessel,^[a, c] Pascal Rusch,^[a, c] Rasmus Himstedt,^[a, c] Daniel Kranz,^[a, c] Hadir Borg,^[a, c] Nadja C. Bigall,^[a, b] and Dirk Dorfs*^[a, b]

Abstract: Investigations on gold and gold-zinc oxide nanocrystals encapsulated in a matrix of a metal-organic framework (ZIF-8) upon plasmonic heating with nanosecond laser pulses are presented. Irradiation of Au@ZIF-8 composite particles leads to heating of the gold core and decomposition of surrounding matrix acting as temperature probe. Cavities inside the ZIF-8 matrix are found on TEM images after irradiation. Their size is determined dependent on laser energy density and the generated heat at the gold core after

absorption of a laser pulse approximated. The surrounding of the gold cores can be heated up to ZIF-8 decomposition over a distance up to 60 nm. This represents a method to visualize heat transfer from the gold cores to the ZIF-8 matrix in three dimensions. Studies on ZIF-8 encapsulated Au@ZnO dot-rod particles give insight in heat transfer between the particle components and show the applicability of the method to different, more complex systems.

Introduction


The encapsulation of nanoparticles in metal organic frameworks (MOFs) has gained a lot of interest in the recent years in several different fields such as sensing,^[1–3] catalysis,^[1,4–7] drug delivery and medicinal chemistry.^[1,8,9] The combination of two functional nanomaterials in one composite particle opens the door for a wide range of possible uses in further fields. Apart from conventional (photo-)catalysis^[10] on nanoparticle surfaces, the laser induced catalysis on optically active nanoparticles has emerged as new field which is centered around the idea of an effective localized activation of the catalytically active nanoparticles by short intense pulses of suitable adjusted laser light.^[11–13] Especially the localized heating of magnetic materials by magnetic hyperthermia or plasmonic active materials like spherical metal nanoparticles, anisotropic metal nanoparticles of various shapes (nanorods,^[14] nanostars,^[15] triangular nano-


platelets, nanocubes and more) and alternative plasmonic materials^[16] by the intense collective oscillation of their charge carrier densities, known as localized surface plasmon resonance (LSPR), could be a possible energy efficient alternative method for the performance of heat driven reactions. Processes directly at the heated nanostructures without the need of heating the complete reaction medium could be realized by exciting the nanoparticles directly with laser light through a translucent medium. The usability and possible parameters of laser induced localized heating of nanocrystals is the focus point of the investigations in our study. We want to gather information about which temperature ranges are achievable in the vicinity of locally heated nanoparticles and where possible destruction thresholds of the heating elements are located. Therefore, we are encapsulating the plasmonic nano heaters (gold nanocrystals in this case) as core elements within a metal organic framework matrix, which itself is not directly affected by the laser irradiation and can act as widely usable temperature indicator (by its decomposition). The resulting effects of the nanosecond laser induced heating on the particles and the indicator matrix are evaluated by transmission electron microscopy, X-ray diffraction and X-ray photoelectron spectroscopy of the irradiated particles.

[a] M. Niemeyer, P. Bessel, P. Rusch, R. Himstedt, D. Kranz, H. Borg, Prof. Dr. N. C. Bigall, Prof. Dr. D. Dorfs
Institute of Physical Chemistry and Electrochemistry
Leibniz Universität Hannover
Callinstr. 3 A, 30167 Hannover (Germany)
E-mail: dirk.dorfs@pci.uni-hannover.de

[b] Prof. Dr. N. C. Bigall, Prof. Dr. D. Dorfs
Cluster of Excellency PhoenixD (Photonics, Optics, and Engineering – Innovation Across Disciplines)
Leibniz Universität Hannover
Welfengarten 1 A30167Hannover (Germany)

[c] M. Niemeyer, P. Bessel, P. Rusch, R. Himstedt, D. Kranz, H. Borg
Laboratory of Nano and Quantum Engineering
Leibniz Universität Hannover
Schneiderberg 39, 30167 Hannover (Germany)

 Supporting information for this article is available on the WWW under <https://doi.org/10.1002/cnma.202200169>

 © 2022 The Authors. ChemNanoMat published by Wiley-VCH GmbH. This is an open access article under the terms of the Creative Commons Attribution Non-Commercial License, which permits use, distribution and reproduction in any medium, provided the original work is properly cited and is not used for commercial purposes.

Results and Discussion

Pulsed Laser Heating of Encapsulated Gold Nanocrystals

The analysis of the area around the heated nanoparticles needs a probe system which is capable to provide not only temperature or information about destructive effects but also positional information. For these means, long chained molecules directly bound to the particle surface with a (temperature)-sensitive moiety in a defined distance from the particle surface are used in the literature to introduce the positional information

into the probe system.^[13,17] We decided to use a different approach by embedding the heatable nanoparticles into a material which is on the one hand not directly affected by the heating method (the incoming laser pulses at 532 nm) and on the other hand has a known thermal degradation temperature. A material which meets these demands and is known to be grown easily on metallic nanoparticles is the metal organic framework ZIF-8 consisting of

the methylimidazolate ion as linker and the zinc(II) ion as SBU (secondary building unit).^[14] Such a composite particle consisting of a semi nano sized ZIF-8 crystal and a gold core in the center of the crystal (see TEM pictures in Figure 1C and 1D), which is capable to be heated by plasmonic heating through an intense laser pulse, can deliver information about the effects affecting its surrounding when the core reaches high temperatures. In advance to the mentioned ligand based approach, the positional information can be evaluated in three dimensions and can give a picture on the spatial evolution of the temper-

ature field or destructive effects induced at the heated gold cores. As shown in Figure 1A, the absorption spectrum of a typical sample of the composite particles we used in this study still shows the characteristic plasmon absorption peak for spherical gold nanoparticles at 532 nm. The presence of gold inside the ZIF-8 crystals can also be confirmed by X-ray diffraction and X-ray photoelectron spectroscopy (see Figures 10–14 in the ESI). The plasmonic feature of the gold cores cannot be seen in extinction measurements because of the scattering caused by the ZIF-8 crystals. Even though a large fraction (about 60% for a whole particle sample, see Figure 3 in the ESI) of the incoming laser light will be scattered by the ZIF-8 matrix before it can reach the plasmonic gold core, it is still possible to excite the core and it can be heated. When the energy density of the incoming light is sufficiently high, as in the laser pulses we are using in this study, the not scattered fraction of the laser energy is still high enough to induce very intense heating effects at the gold cores. As shown in Figure 1B

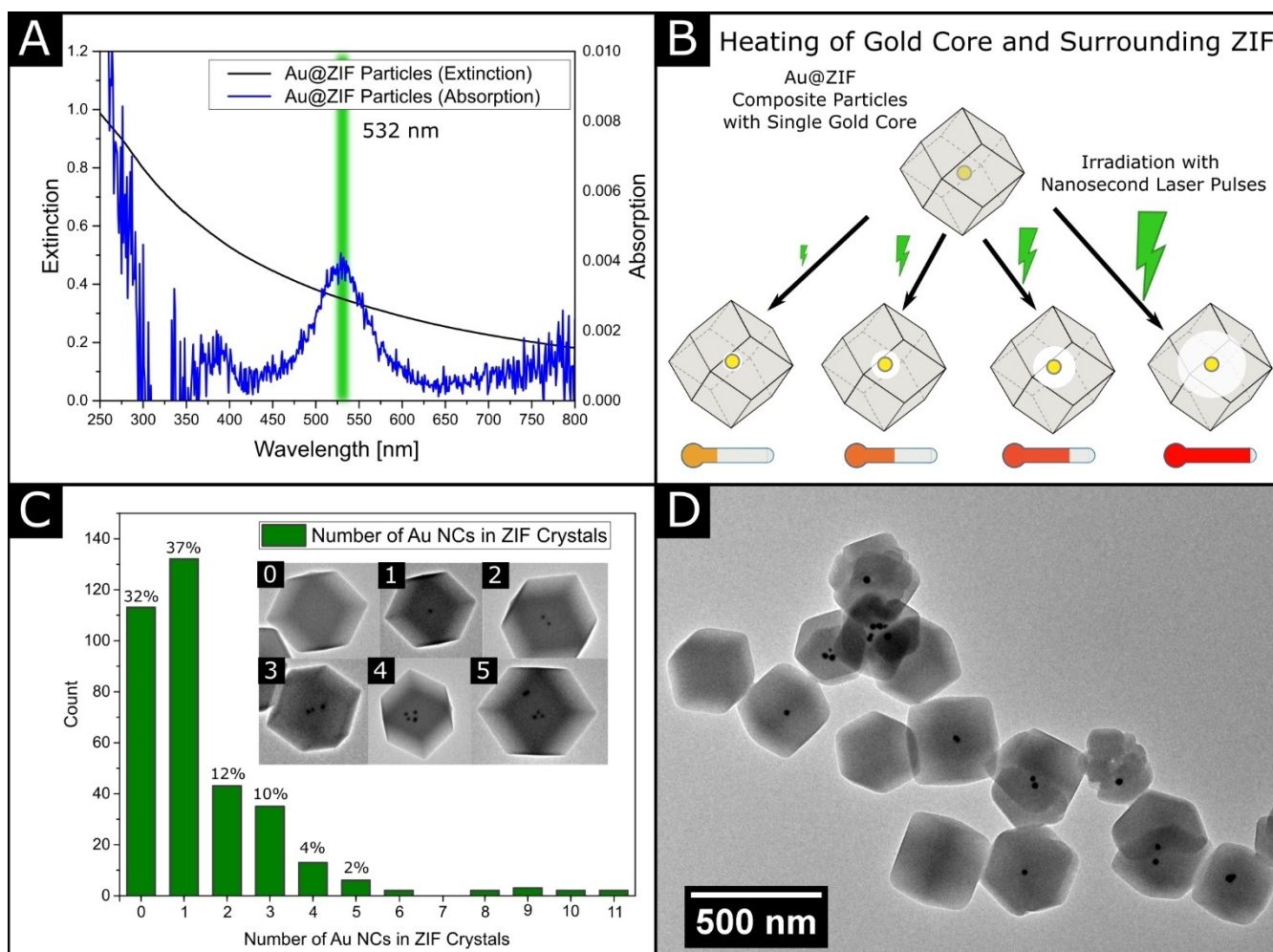


Figure 1. (A): The composite Au@ZIF-8 particles show a spectrum in UV-Vis extinction measurements with a high fraction of scattering (black curve). Absorption measurements reveal the characteristic plasmonic feature which can be excited with laser pulses at 532 nm. (B): The excitation of the plasmonic active gold cores inside the ZIF-8 matrix leads to plasmonic heating of the cores which results in the formation of cavities inside the composite particles. Depending on the used laser energy density, the size of the cavities can be varied. (C): Core particle number distribution of the composite particles. For an adequate determination of the cavity diameter the composite particles ideally should show one core particle which is the case for most particles in the samples. (D): TEM picture of a sample of the synthesized Au@ZIF composite particles.

schematically the ZIF-8 around the heated gold core is being removed by thermal degradation or different destructive effects and cavities form, which can be found by the examination of TEM images of the irradiated particle samples. The gold cores absorb more energy and emit larger amounts of heat the higher the laser energy densities are. Therefore, more ZIF-8 material should be transformed to zinc oxide (as can be concluded from TG measurements) and organic fragments resulting in larger cavities. To investigate this effect, we made a series of irradiation experiments with laser energy densities ranging between $20 \text{ mJ}\cdot\text{cm}^{-2}$ and $700 \text{ mJ}\cdot\text{cm}^{-2}$ on identically prepared samples of composite particles with mostly one gold core per ZIF-8 nanocrystal. As it can be seen from the TEM pictures in Figure 2, the formation of detectable cavities around the gold cores seems to start between a energy density of $20 \text{ mJ}\cdot\text{cm}^{-2}$ and $35 \text{ mJ}\cdot\text{cm}^{-2}$. The pictures of the samples irradiated with $20 \text{ mJ}\cdot\text{cm}^{-2}$ show no noticeable difference to the pictures of the not irradiated samples. When $35 \text{ mJ}\cdot\text{cm}^{-2}$ are used, small areas with a brighter contrast around the gold cores in the ZIF nanocrystals can be identified as cavities in the material. As expected, these cavities have a slightly larger diameter than the mean diameter of the gold cores. The size and also the length of the cavities increases slightly when the

laser energy density is raised stepwise. At energy densities in the range of $35 \text{ mJ}\cdot\text{cm}^{-2}$ to $140 \text{ mJ}\cdot\text{cm}^{-2}$ the gold cores seem to reach a temperature which is critical for their structural stability. When the TEM pictures of samples irradiated with energy densities larger than $140 \text{ mJ}\cdot\text{cm}^{-2}$ are evaluated, it is not possible to find the original gold cores of about 25 nm size inside the cavities anymore. Accordingly, the mean particle diameter of the gold cores is decreasing rapidly from the pristine size of 25 nm to about 5 nm in this energy density interval (see Figure 3A).

Therefore, it is likely that at the gold cores temperatures in the range of the melting point of bulk gold were induced and they splintered into lots of smaller pieces and gold ions (coulomb explosion).^[18] Since these pieces were still heated to very high temperatures they were able to burn through the MOF material and reach the outside of the nanocrystals. Besides that, the cavities are in most cases spherical but can also be elongated and tunnel-shaped. As shown in Figure 3B, often the tunnels have diameters which are quite large in the middle of the ZIF-8 crystals and are getting smaller further away from the middle of the crystals. This is a hint for a loss of heat of a hot gold core which has been hit by a laser pulse and is cooling down while it is moving inside the crystal, forming the tunnel-like structure. Due to its temperature the amount of MOF which is decomposing around its surface is reducing with time the longer it moves through the crystal. Similar observations can be made for every further sample which has been irradiated with energy densities between $140 \text{ mJ}\cdot\text{cm}^{-2}$ and $700 \text{ mJ}\cdot\text{cm}^{-2}$. Comparable results could also be observed by OSAKA *et al.* at laser excited gold nanoparticles on glass substrates.^[19] They were able to heat the glass substrates to their melting point via the heated nanoparticles which cut tunnel like structures into the material. EDX measurements on irradiated and not irradiated samples (See Figures 6–9 in the ESI) indicate that the

linker-SBU structure of the metal organic framework is still intact in the regions far away from the gold cores after the laser irradiation. The investigation with X-ray diffraction and XPS measurements (see SI Figures 10–14) indicates that the formation of small amounts of other materials like zinc nitrate or AuZn alloy takes place due to the induced heat at the gold cores. But it can be confirmed that the ZIF structure remains mostly intact in the remaining material. To quantify the relation between the used laser energy density and the resulting cavity size, the samples were examined by transmission electron microscopy so that at least 40–50 size-measurements of the resulting cavities for each used laser energy density could be made. For the size distributions at each laser energy density see Figures 4 and 5 in the ESI. According to the approximately spherical shape of the cavities, the evolution of the cavity radius with rising laser energy density can be fit roughly to a cubic root function (see Figure 3C). Which is in unison with the assumption that the evolving Volume in which the ZIF-8 matrix is affected by the destructive effects induced by the laser irradiation is evolving around the spherical gold cores of the composite particles and scales approximately linearly with the increasing laser energy density (Figure 3D).

This finding is particularly interesting as it seems to be valid even far beyond the laser intensities which are necessary to destroy the gold nanoparticles. This indicates, that even when the light absorbing gold particles are completely destroyed by the laser pulse, still most of the generated heat is very strongly confined to the original position of the gold particle.

Estimation of Absorbed Heat

The Energy which is needed to decompose the amount of ZIF-8 which was located in the formed cavities can be determined by the estimation of the molar amount of ZIF-8 and its molar decomposition enthalpy. The latter one can be roughly determined via thermogravimetric measurements. This method of estimation is based on several simplifying assumptions: First, due to the very different heating rates upon laser induced heating and heating in TG analysis, it is not clear if the same reaction products are obtained. Therefore the decomposition enthalpy might also differ in both experiments. Secondly, the solvent (MeOH) used in the irradiation experiments might also have an influence on the heated components. Third, the formation of nano bubbles, shock waves and expansion of high temperature gas also become non-negligible effects in the regime of about $100 \text{ mJ}\cdot\text{cm}^{-2}$ laser energy density.^[20] Therefore these effects begin to have an impact on the cavity size because of their additional destructive nature concerning the ZIF-8 matrix and the accuracy of the heat estimation diminishes with increasing energy density. However, we still find a linear rise of the cavity volume also in this regime (within the admittedly large margin of error).

To estimate the molar decomposition enthalpy of the ZIF-8 nanocrystals under conventional heating conditions in thermogravimetric measurements, these were synthesized and prepared as described in the experimental section. The resulting

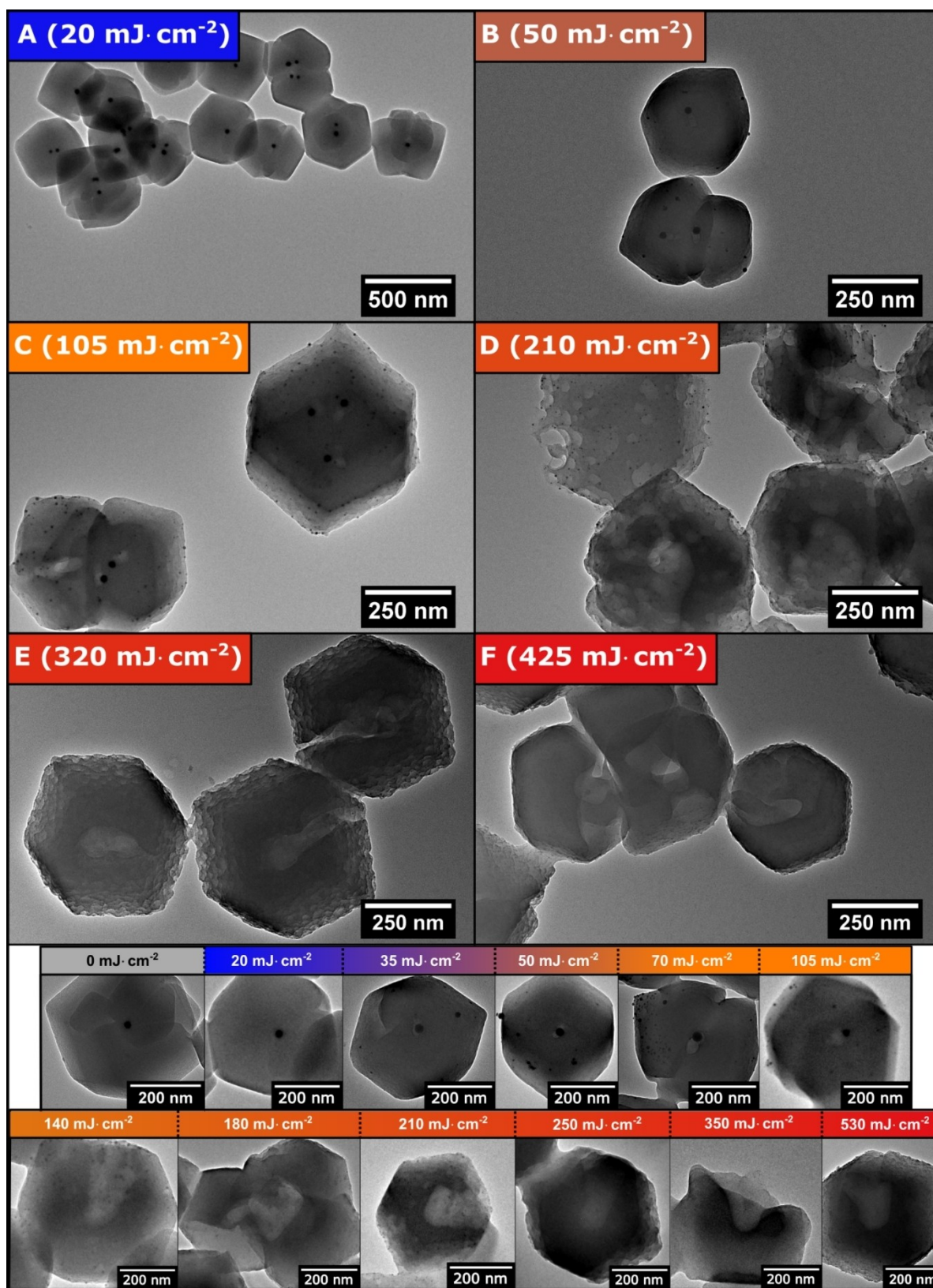


Figure 2. (A–F): TEM pictures taken from samples of Au@ZIF-8 composite particles irradiated at several different laser energy densities confirm the formation of cavities around the gold cores and the size dependency of the cavities on the used laser irradiation. The gold cores seem to disintegrate when laser energy densities higher than 105 mJ·cm⁻² are used and instead many very small gold particles can be found (D–F).

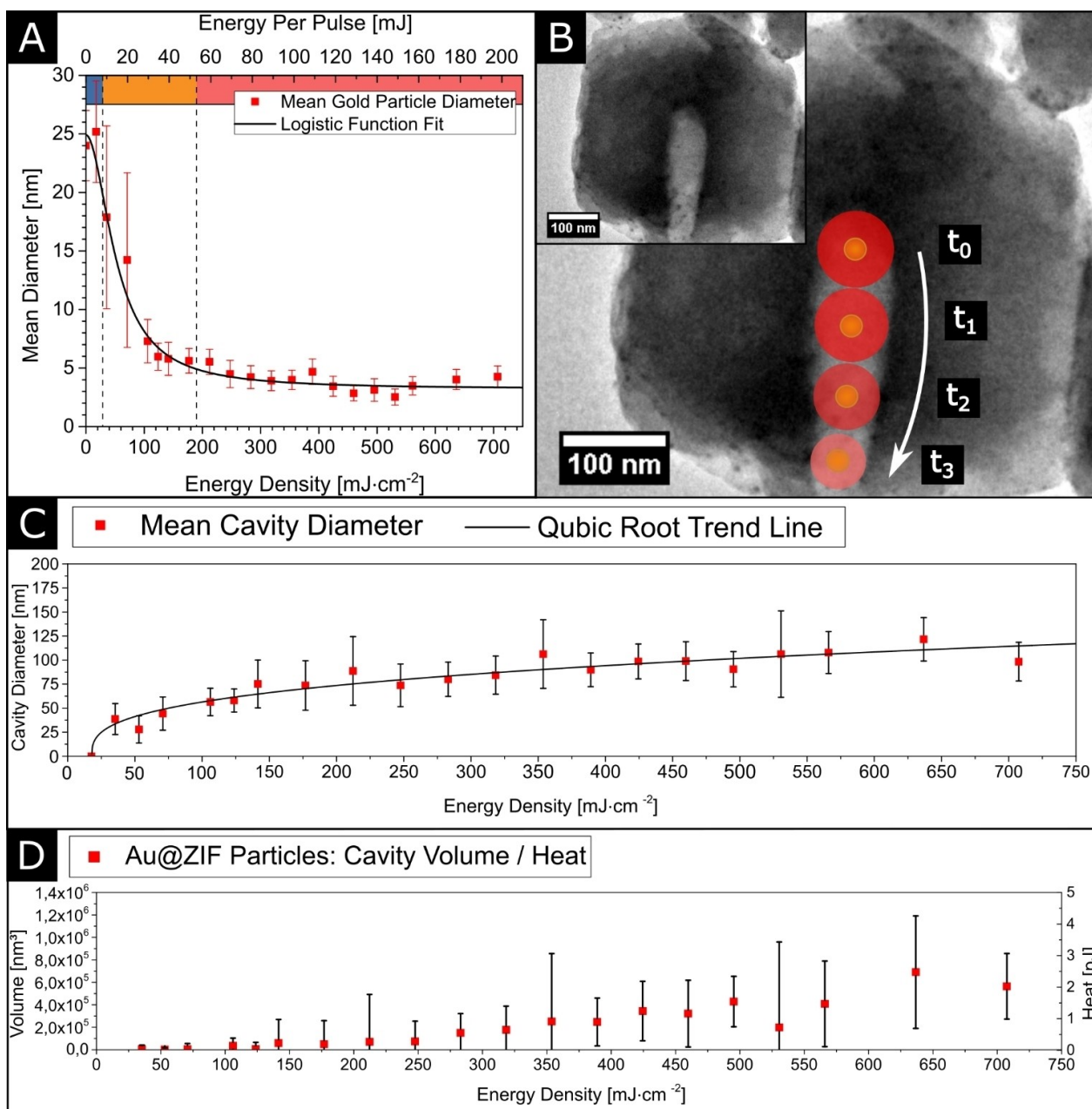


Figure 3. (A): Correlation between gold particle size after irradiation and used laser energy density from the evaluation of several TEM pictures for each energy density respectively. (B): Schematic representation of the tunnel formation mechanism inside the ZIF-8 crystals by the heated gold particles. (C): Correlation between laser pulse energy density and cavity diameter (and calculated spherical volume in (D)) obtained by the evaluation of several TEM pictures for each respective laser energy density.

mass loss and heat flow curves are shown in Figure 4. The data from these measurements and the obtained cavity volumes can be used to calculate the heat values corresponding to a given cavity volume as described in the SI. These values are included in Figure 3D via a second y-axis. This leads to the conclusion that the gold cores are capable of the absorption and transmission of relatively large amounts of energy in the range of several picojoules per particle from the incoming laser pulses to the close vicinity in the surrounding material. Which equals approximately $3,2 \text{ MJ}\cdot\text{mol}^{-1}$ of gold atoms and is one

magnitude higher than the Au–Au bond energy of $220 \text{ kJ}\cdot\text{mol}^{-1}$.^[21] So this energy likely can be used for temperature induced processes near the particles surface.

Estimation of Temperature and Temperature Distribution

Laser Energy densities between $20 \text{ mJ}\cdot\text{cm}^{-2}$ and $80 \text{ mJ}\cdot\text{cm}^{-2}$ are in the range which are correlated with melting or shape changes of non-spherical gold nanostructures in the

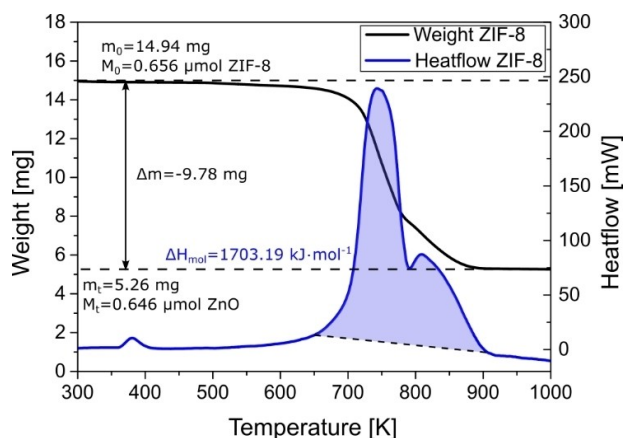


Figure 4. Thermogravimetric mass loss curve (black line) and heat flow curve of the differential scanning calorimetry measurements (blue curve) made on ZIF-8 nanocrystals.

literature.^[22,23] For gold nanoparticles of 38 nm a melting temperature of about 1000 K is reported under conventional heating. Respective shape changes of non-spherical particles could occur at even lower temperatures (673 K).^[23,24] These findings from other groups and the observation that the thermal decomposition temperature of the ZIF-8 matrix (750 K, see Figure 4) and the formation temperature of AuZn (1024 K) (see Figure 10 in the ESI) have been reached in the particles surrounding, give rise to the assumption that temperatures in this range were induced by the laser pulses at the particles. Calculations and transient absorption spectroscopy related experiments by other groups suggest that temperatures of 2000–3000 K of nanosecond laser irradiated gold nanoparticles of about 30 nm size are possible in the energy density region beginning at $60 \text{ mJ} \cdot \text{cm}^{-2}$.^[25] With regards to possible fragmentation by coulomb explosions or surface evaporation of the irradiated gold cores at these temperatures, the beginning decrease of the mean gold particle size as shown in Figure 3 in the same energy density regime is plausible. With increasing

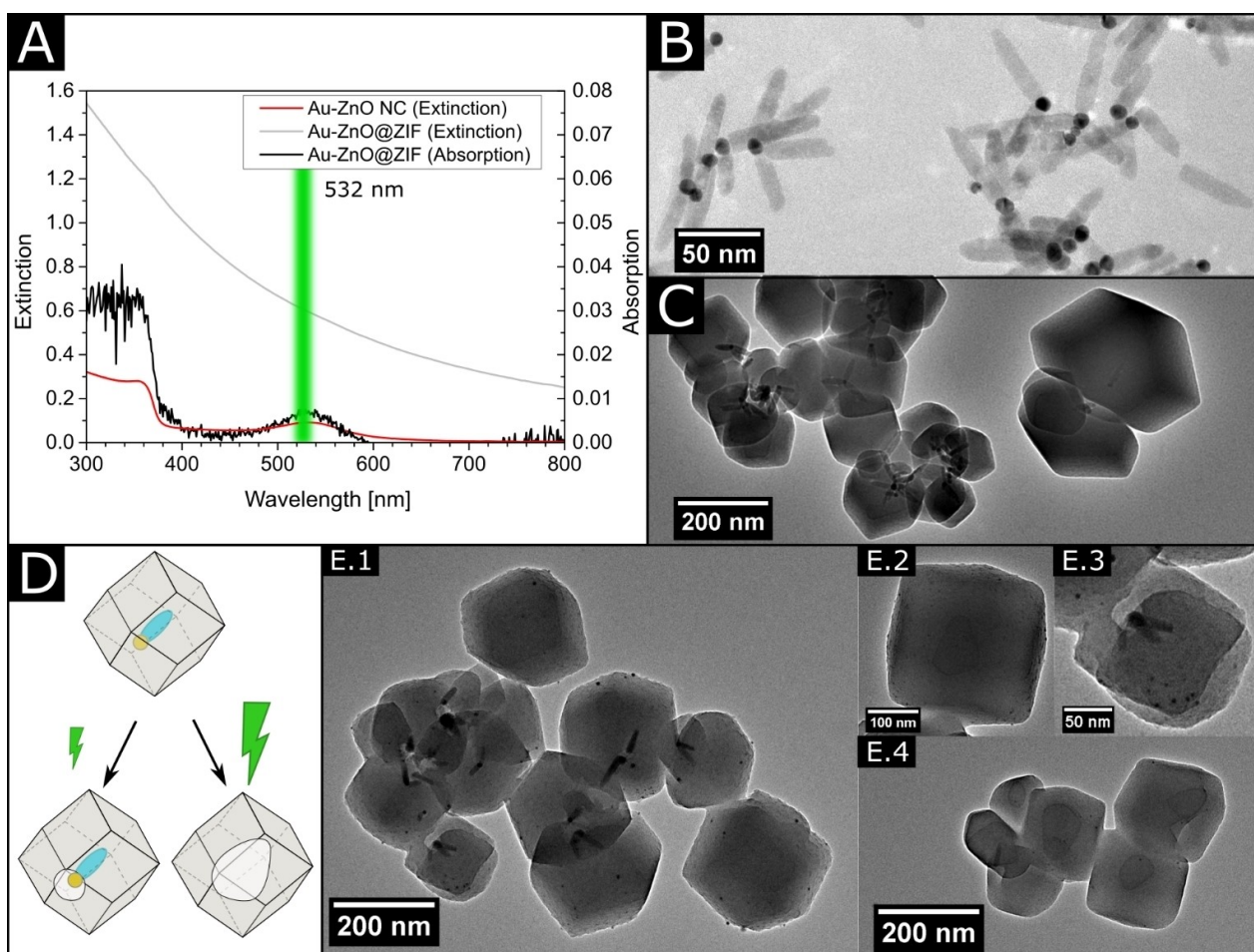


Figure 5. (A): Extinction and absorption spectra of the Au-ZnO particles and the encapsulated Au-ZnO@ZIF-8 particles. The indicated laserline matches the plasmonic feature of the gold component at 532 nm. (B): TEM pictures of the as synthesized Au-ZnO nanoparticles and the Au-ZnO@ZIF-8 particles (C). (D): Schematic representation of the composite Au-ZnO@ZIF-8 particles before and after laser irradiation. The formed cavities have the elongated shape of the complete hetero Au-ZnO particles at high energy densities. (E.1 and E.3): TEM Pictures of Au-ZnO@ZIF-8 particles irradiated with low energy density ($35 \text{ mJ} \cdot \text{cm}^{-2}$). Cavities around the gold component of the Au-ZnO particles can be found. (E.2 and E.4): TEM pictures of the same particles irradiated with a high energy density ($250 \text{ mJ} \cdot \text{cm}^{-2}$). The cavities match the shape of the former encapsulated Au-ZnO hetero particles.

energy density, the mean particle size decreases steadily until only very small particles of about 5 nm size can be found beginning at about $140 \text{ mJ}\cdot\text{cm}^{-2}$ of laser energy density (See Figure 3A). Also it can be assumed by the examination of the TEM pictures, showing no original sized gold cores anymore, that the effects causing the fragmentation become more and more prominent. Plasma formation and temperatures in the regime of 10000 K are mostly reported only for ultra short pulses below the nanosecond regime and energy densities of over $1 \text{ J}\cdot\text{cm}^{-2}$ which are used in typical laser ablation experiments.^[26] But these reports are mostly referring to experiments with bulk gold substrates. So if and at which laser energy densities plasma formation and the transition to the critical state could also be reachable on nanoparticles in solution or in a matrix at lower intensities remains speculative. Therefore the respective temperatures in the energy density range beginning at $140 \text{ mJ}\cdot\text{cm}^{-2}$ must be clearly below 10000 K and above 3000 K. In conclusion the temperatures in this region maybe be located in the regime between 3000 K and 6000 K.

In the Region of $20 \text{ mJ}\cdot\text{cm}^{-2}$ to $80 \text{ mJ}\cdot\text{cm}^{-2}$ the average cavity radius can be estimated to be at 15–25 nm (see Figure 3C). For an estimation of the temperature distribution around a laser heated gold core, the average radius of a gold core (13 nm) can be subtracted. The resulting length ($R_T = 2\text{--}12 \text{ nm}$) represents the distance between the outer edge of the cavity and the particle surface. Within this distance the temperature of the particle surface must have been decayed from about 1000 K to the decomposition temperature of ZIF-8 (750 K) and below. When the laser energy density is raised to a level of $140 \text{ mJ}\cdot\text{cm}^{-2}$ ($T > 3000 \text{ K}$) the R_T distance increases up to 25 nm. At the highest used laser intensity of $710 \text{ mJ}\cdot\text{cm}^{-2}$ ($T < 10000 \text{ K}$) a distance of 45 nm can be calculated.

The temperature differences at the gold cores are theoretically decaying to the decomposition temperature of ZIF-8 at 750 K over a range of approximately 10–45 nm depending on the laser energy density, leads to the assumption that the corresponding temperature profiles around the heated gold cores must be very steep. This underlines that the cooling effects of the surrounding medium must have a large influence on the thermal evolution at these scales and in these time regimes even at very high temperatures. These findings suggest that a repeated use of such nano heating systems is limited to laser energy densities below $100 \text{ mJ}\cdot\text{cm}^{-2}$ and a distance to the heating element within approximately 10 nm. Above these laser energy densities, the structural integrity of the gold cores is not given anymore.

Irradiation of Au-ZnO@ZIF-8 Composite Particles

In analogy to the experiments with composite particles with only a gold particle encapsulated inside the ZIF-8 nanocrystals, we synthesized, encapsulated and irradiated gold zinc oxide hetero particles (Figure 5B) in the ZIF-8 crystals (Figure 5C) to investigate the heat transfer from the heated gold cores over the zinc oxide component to the ZIF-8 matrix. As the UV-Vis spectra in Figure 5A indicate, the plasmonic feature of the gold

component is not visible in extinction mode due to the strong scattering of the ZIF-8 crystals, just as reported for the composite particles only with the gold cores. Similar as observed for these particles, the Au-ZnO@ZIF-8 particle samples reveal the spectral features of the bare hetero Au-ZnO particles in absorption measurements. The plasmonic resonance matches the used laser wavelength for the irradiation experiments while the band gap absorption feature is not affected by the laser wavelength and therefore the zinc oxide component cannot be heated directly by the laser pulses. As for the Au@ZIF composite system the presence of Au-ZnO particles inside the ZIF material can be confirmed by X-ray diffraction and XPS measurements (see Figures 10 in the ESI). Now it can be observed by the examination of TEM pictures that the cavities in the ZIF-8 matrix are also forming when the encapsulated Au-ZnO hetero particles are irradiated. Figure 5E.1 shows a sample irradiated with $35 \text{ mJ}\cdot\text{cm}^{-2}$. Small cavities only around the gold component of the hetero Au-ZnO particles can be found, which is in unison with the observations made for the composite particles only with the gold cores. The zinc oxide component seems not to be heated strong enough to decompose its surrounding ZIF-8 material and therefore no cavities can be observed around this component at these energy densities like indicated in the scheme in Figure 5D. In contrast to these observations, the TEM pictures obtained after irradiation of the same particles with an energy density of $250 \text{ mJ}\cdot\text{cm}^{-2}$ (Figure 5E.4) show cavities which are elongated and match the shape of the whole former encapsulated Au-ZnO hetero particles. This gives rise to the assumption that at these energy densities the heat, which is evolving at the irradiated gold cores, can be transferred to the directly attached zinc oxide component before the surrounding ZIF-8 matrix with a very low thermal conductivity ($0.165 \text{ W}\cdot\text{m}^{-1}\text{K}^{-1}$)^[27] compared to gold ($314 \text{ W}\cdot\text{m}^{-1}\text{K}^{-1}$)^[28] and zinc oxide ($43 \text{ W}\cdot\text{m}^{-1}\text{K}^{-1}$)^[29] is being affected by any destructive effect. Also at higher irradiation energy densities the absorbed energy seems to be large enough to destroy both components of the hetero particle and even a fraction of the ZIF-8 matrix around them. The method provides clear evidence, that heterostructured nanocrystals can selectively and regional confined be heated (gold component) by the choice of incoming laser energy density and that the induced heat is being transferred directly to the attached component (zinc oxide rod) when the laser energy density is being raised. This is to our knowledge the first application of an experimental method to visualize the effects of fast laser heating on hetero structured nanocrystals in three dimensions. The very low heat conductivity of the ZIF-8 matrix is ideal to monitor heat conduction within encapsulated structures. It enables the method to be applicable to the exploration of the heat conductive behavior of multi component nanostructured systems. Including a wide range of other materials as other oxide or sulfide types combined with plasmonic noble metal particles for the final use as drug delivery systems or nano sized catalysts in which the MOF material also could act as size selective filter unit.^[30–32]

Conclusion

We synthesized ZIF-8 nanocrystals with mostly one plasmonic gold core inside and gold zinc oxide hetero particles encapsulated in ZIF-8 nanocrystals. To investigate the thermal behavior of the gold cores under irradiation with nanosecond pulsed visible laser light, we performed irradiation experiments of the particles in solution using several different laser energy densities. By the evaluation of TEM pictures of the irradiated samples, we found that the irradiation of the gold cores resulted in cavities in the ZIF-8 matrix observable at the positions of the gold cores. This leads to the assumption that the absorbed energy induced laser driven plasmonic heating of the gold components. The generated temperatures are also high enough to decompose the ZIF-8 matrix around them partially in defined areas. The comparison of TEM pictures taken after irradiation at different energy densities shows that the decomposed areas of ZIF-8 are getting larger when the laser energy density is raised. Furthermore, we approximated the amount of heat which evolved at the plasmonic heated gold cores by the estimation of the accumulated decomposition energy of the removed ZIF-8 material. We could also confirm that the ZIF-8 matrix is only affected in the cavity areas. Apart from the formed cavities the ZIF-8 material seems to remain intact. The observation that the ZIF-8 matrix is being destroyed in defined areas while the heated gold cores remain intact, underlines the presence of a confined heating effect. In an area of 10 to 45 nm (depending on the laser energy density) around the irradiated gold cores at least the degradation temperature of the matrix of 750 K is reached. The experiments with the Au-ZnO hetero particles inside the ZIF-8 matrix confirm these confined heating effects and in addition they deliver hints for a heat transfer from the heated gold cores to the zinc oxide component before the ZIF-8 matrix is being affected and show the applicability of this heat monitoring method to different materials and more complex structures. With these insights we contribute to a possible parameter range concerning reachable temperatures, respective usable laser energy densities as also a destruction threshold for the used gold particles (especially inside a metal organic framework matrix) as laser driven plasmonic nano heaters for thermal induced processes, which find their application mostly in drug delivery systems and catalysis.

Experimental Section

All chemicals were obtained from commercial suppliers and used without further modifications. hydrogen tetrachloroaurate(III) trihydrate 99,99% (Alfa Aesar); methanol 99.8% (Sigma Aldrich); ethanol 99.8% (Sigma Aldrich); hexane 99.8% (Sigma Aldrich); zinc nitrate hexahydrate >99% (Sigma Aldrich); 2-methylimidazole 98% (Sigma Aldrich); polyvinylpyrrolidone (PVP; $M_w = 55.000$) (Sigma Aldrich); trisodium citrate dihydrate 99.0% (ABCR) Water was distilled and filtered by an in house distillation unit.

Synthesis of PVP Coated Gold Nanoparticles^[33]

The Synthesis was done following the procedure by HUPP, HUO et al. a 0.01 wt% aqueous solution of HAuCl_4 (50 mL, 15 nmol) were heated to reflux in a 100 mL flask. Subsequently 1 wt% sodium citrate solution (1.5 mL, 60 nmol) was added and the reaction mixture was held under reflux and stirred on 800 rpm for 20 min. Subsequently the reaction mixture was cooled down to room temperature. Separately a solution of polyvinylpyrrolidone (PVP; $M_w = 55.000$, 10 mL, 0.1666 g) and distilled water was prepared by dissolving the PVP by heating the mixture in a 20 mL vial to 313 K. Subsequently the PVP solution was added drop wise over 20 min ($0.5 \text{ mL} \cdot \text{min}^{-1}$) under stirring to the flask with the nanoparticle solution by the use of a syringe pump (type Landgraf LA-120). The particle/PVP mixture then was stirred for 24 hours at 400 rpm at room temperature (293 K). The resulting particles were washed by the centrifugation of 2 mL portions at 14000 rpm ($14100 \times g$) for 30 min. After centrifugation the particles were re dispersed in methanol (2 mL) the washing procedure was repeated two additional times. Finally the particles were stored in methanol.

Synthesis of PVP Coated Au-ZnO Nanoparticles^[32]

For the synthesis of gold nanospheres with attached zinc oxide rods the synthesis procedure by TAHIR et al. was adopted: In a one-pot synthesis auric acid (HAuCl_4 , 20 mg, 0.05 mmol) was mixed with $\text{Zn}(\text{NO}_3)_2 \times 2\text{H}_2\text{O}$ (109 mg, 0.5 mmol), 1-octadecene (2.5 mL), phenyl-methanol (5 mL) and oleylamine (3 mL) in a 25 mL three necked flask until the solids were mixed. The mixture was heated to 393 K with a heating rate of $5 \text{ K} \cdot \text{min}^{-1}$ and held at this temperature for more 20 min. Then the temperature was raised up to 453 K with the same heating rate and held at this temperature for 30 min. After the reaction was finished the mixture was cooled down to room temperature and of ethanol (16 mL) was added. After centrifugation at 6000 rpm ($3421 \times g$) for 10 min, the particles were redispersed in chloroform (14 mL) and the washing procedure was repeated twice. For the PVP coating 10 mL of a PVP solution were prepared and used with 5 mL of the particles in chloroform as described in the section for the synthesis of PVP coated gold nanoparticles. After the coating finished Hexane (0.4 mL per mL) solution was added and the solution was centrifuged at $13400 \times g$ for 10 min and redispersed in methanol two times.

Synthesis of ZIF-8 Nanoparticles^[33]

For a typical synthesis of ZIF-8 nanocrystals 2-methylimidazole (2-mim, 2.5 mL, 1.8 mg, 0.022 mmol) and Zinc Nitrate ($\text{Zn}(\text{NO}_3)_2 \times 2\text{H}_2\text{O}$, 2.5 mL, 5 mg, 0.022 mmol) methanolic solutions were prepared and mixed in a 8 mL vial by shaking for 5–10 seconds. Subsequently the solution was standing undisturbed at room temperature (293 K) for 24 hours. To wash the resulting particles the solutions were centrifuged at 6000 rpm ($3421 \times g$) for 5 min and redispersed in methanol (3 mL). The washing procedure was repeated 3 times. Finally the particles were stored in methanol.

Synthesis of Single Core Au@ZIF-8 Composite Particles^[33]

For the synthesis of composite Au@ZIF-8 particles with only one gold core, methanolic solutions of 2-Methylimidazole (2-mim, 2.5 mL, 1.8 mg, 0.022 mmol) and Zinc Nitrate ($\text{Zn}(\text{NO}_3)_2 \times 2\text{H}_2\text{O}$, 2.5 mL, 5 mg, 0.022 mmol) were prepared. For a typical batch 2.5 mL of the 2-mim solution were filled in a 8 mL vial and 20 μL of gold particle solution with a concentration of $4 \text{ nmol} \cdot \text{L}^{-1}$ (estimated with the molar extinction coefficient for 25 nm sized gold particles),^[34] were added and the Mixture was shaken by hand for

5–10 seconds. Then 2.5 mL of the prepared zinc nitrate Solution were added to the reaction mixture and the vial was shaken again for 5–10 seconds. Then the mixture was standing undisturbed at room temperature (293 K) for 24 hours. To wash the resulting particles, the solution was centrifuged at 5000 rpm (3421 \times g) for 5 min and redispersed in methanol (3 mL). The washing procedure was repeated 3 times. Finally, the particles were stored in methanol.

Synthesis of Au-ZnO@ZIF-8 Composite Particles

For the encapsulation of the Au-ZnO particles in ZIF-8 nanocrystals 10 μ L of the particles in methanol were added to a methanolic solution of 2-mim (5 mL, 12.3 mg, 0.15 mmol) in a 30 mL vial. After the solution was placed in an ultrasonic bath for 5 min, a methanolic solution of zinc nitrate (5 mL, 33.8 mg mg, 0.15 mmol) solution was added rapidly and the vial was shaken for several seconds. Then the solution was left undisturbed for 24 hours. The resulting particles were washed as described in the section for the Au@ZIF-8 composite particles.

Laser Irradiation Experiments

500 μ L of the synthesized composite Au@ZIF particles were mixed with 1.5 mL methanol in a 3 mL cubic cuvette with a path length of 1 cm by Hellma Analytics equipped with a stirring bar. The cuvette was placed in the cuvette holder of the laser setup which is shown in Figure 6.

The energy density of the passing laser pulses was modified by the use of neutral density filters positioned in front of the cuvette holder and the variation of the voltage of the flash lamp of the laser head. To measure the laser energy density, the setup was equipped with a pyroelectric energy meter positioned behind the cuvette holder. To prevent segregation of the particles while the irradiation experiments the particle solution was stirred inside the

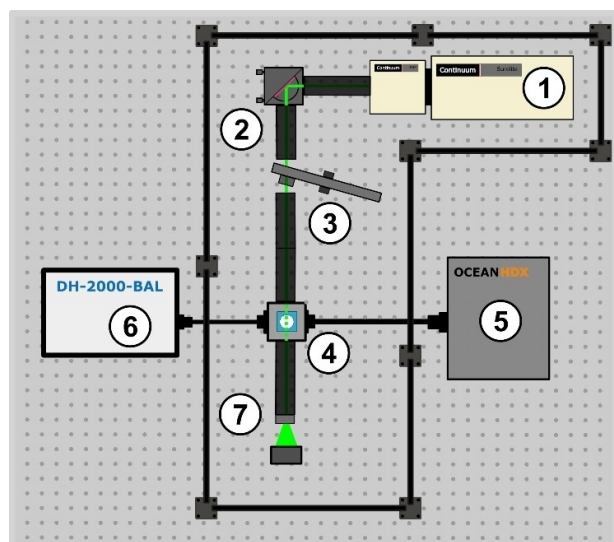


Figure 6. Schematic of the Laser Setup. The beam from the Continuum SL–Nd:YAG laser (1) is reflected by a laser line mirror (2) and directed through a filter wheel with neutral density filters (3) and afterwards through the sample in the cuvette holder (4). The cuvette holder is connected to a HDX UV-Vis spectrometer (5) with a BAL-2000 light source (6) by Ocean Optics via fibre cables on a second optical axis. Finally, the beam is spread to a diameter of 5 cm by a lens and hits a pyroelectric Energy Max J-25MT T-10KHz energy sensor (7) by Coherent.

cuvette. In a typical experiment the samples were irradiated with 10000 Pulses at a pulse frequency of 10 Hz with a wavelength of 532 nm.

Thermogravimetric and Differential Scanning Calorimetry Measurements

For the thermogravimetric (TG) and differential scanning calorimetry analysis of the ZIF-8 nanoparticles 14 mg of precipitated and dried ZIF-8 sample was filled in a small ceramic vessel and put in the autosampler of a TGA/DSC 3+ measuring unit by Mettler Toledo. The measurements were performed under air atmosphere between 300 K and 1000 K with a heating rate of 0.15 K per second. For the evaluation of the measurements the Mettler Toledo software STARe Version 16.20 was used.

Preparation of Transmission Electron Microscopy (TEM) and Energy-dispersive X-ray Spectroscopy (EDX) Samples

TEM samples were prepared by dropping small amounts of nanoparticle solution in methanol on copper grids with 300 mesh by Quantifoil. Between the application of the drops the solvent was being allowed to evaporate. To achieve a good distribution of particles on the grid 3–5 drops were needed for the synthesized particle samples. Because the irradiated particle samples were diluted up to ten fold compared to the synthesized samples, the amount of drops needed for a good distribution was between 25 and 30 drops of irradiated particle solution. The measurements were performed on a Tecnai G2 F20 TMP electron microscope by FEI with a acceleration voltage of 200 kV. The EDX measurements were made with a EDAX Octane T Optima 60 SDD System coupled with the Tecnai microscope.

UV-Vis and Dynamic Light Scattering (DLS) Measurements

Spectroscopic measurements of the particle samples in methanol were performed with the use of 3 mL cubic quartz cuvettes with a path length of 1 cm by Hellma Analytics. The extinction spectra were recorded with the use of a second reference cuvette in the beamline of a Cary 5000 spectrophotometer by Agilent. For the absorption spectra measurements an DRA-2500 integrating sphere accessory for the Cary 5000 by Agilent was used. In most cases the same cuvettes prepared for UV-Vis measurements were also used to perform DLS measurements on a Zetasizer ZSP nano by Malvern Panalytical. The DLS measurements were repeated at least 5 times with 10 sub runs. For the UV-Vis Spectra and DLS size distributions of the composite particles see Figure 1 and Figure 2 in the ESI. The spectra and size distributions of the gold cores can be found in Figure 1 in the ESI.

X-Ray Diffraction (XRD) Measurements

Phase analysis of the core particles and composite particle samples was performed via X-ray diffraction. The samples were prepared by dropcasting the colloidal samples from methanolic solution on silicon wafers. The measurements were made between $2\Theta = 10^\circ$ and $2\Theta = 80^\circ$ with an D8 Advance by Bruker with Bragg-Brentano geometry using 30 kV, a resolution of 0.01° and an integration time of 4 seconds. Reference reflection positions were taken from literature or simulated using the software VESTA^[35] and structure data from the crystallography open database (COD).^[36]

X-Ray Photoelectron Spectroscopy (XPS) Measurements

Analysis of the elemental electron binding energies of the materials of core particles and composite particle samples was performed via X-ray photoelectron spectroscopy with a PHI 5000 VersaProbe III spectrometer (ULVAC-PHI, Chigasaki-shi, Japan) with an Al $K\alpha$ beam source at 1486.6 eV. The samples were prepared by dropcasting the colloidal samples from methanolic solution on slides of ITO-glass. The obtained spectra were compared with reference data from literature.

Acknowledgements

The team of authors would like to thank following people and institutions: D.D. thanks the Deutsche Forschungsgemeinschaft for the DFG Research Grant 1580/5-1. D.D. and N.C.B. are thankful for the funding by the Deutsche Forschungsgemeinschaft (DFG, German Research Foundation) under Germany's Excellence Strategy within the Cluster of Excellence PhoenixD (EXC2122). M.N. is thankful for the financial support by the Graduiertenakademie of the Leibniz University Hanover. P.B. and R.H. are thankful to the Hannover School for Nanotechnology for financial support. D.K. is grateful for funding by the Konrad-Adenauer-Stiftung (KAS). N.C.B. received funding from the European Research Council (ERC) under the European Union's Horizon 2020 research and innovation programme (Grant Agreement No. 714429). The whole team of authors thanks the Labororium of Nano- and Quantum Engineering for supporting work space, laboratories and access to the TEM and Apl. Prof. Armin Feldhoff for access to the XRD device. Open Access funding enabled and organized by Projekt DEAL.

Conflict of Interest

The authors declare no conflict of interest.

Data Availability Statement

The data that support the findings of this study are available on request from the corresponding author. The data are not publicly available due to privacy or ethical restrictions.

Keywords: Plasmonics · Laser Heating · Metal Organic Framework · Composite · Nanoparticles

- [1] G. Zheng, L. M. L. Marzán, I. P. Santos, J. P. Juste, *SmartMat* **2021**, *2*, 446.
- [2] D. Wang, Z. Li, J. Zhou, H. Fang, X. He, P. Jena, J. Bin Zeng, W. N. Wang, *Nano-Micro Lett.* **2018**, *10*, 1.
- [3] L. E. Kreno, J. T. Hupp, R. P. Van Duyne, *Anal. Chem.* **2010**, *82*, 8042.
- [4] A. Dhakshinamoorthy, A. M. Asiri, H. García, *ACS Catal.* **2017**, *7*, 2896.
- [5] R. Wu, X. Qian, K. Zhou, H. Liu, B. Yadian, J. Wei, H. Zhu, Y. Huang, *J. Mater. Chem. A* **2013**, *1*, 14294.
- [6] X. Yang, L. Qiu, X. Luo, *RSC Adv.* **2018**, *8*, 4890.

- [7] Y. K. Park, S. B. Choi, H. J. Nam, D. Y. Jung, H. C. Ahn, K. Choi, H. Furukawa, J. Kim, *Chem. Commun.* **2010**, *46*, 3086.
- [8] Y. Li, J. Jin, D. Wang, J. Lv, K. Hou, Y. Liu, C. Chen, Z. Tang, *Nano Res.* **2018**, *11*, 3294.
- [9] H. Zhang, Q. Zhang, C. Liu, B. Han, *Biomater. Sci.* **2019**, *7*, 1696.
- [10] L. Chen, Y. Peng, H. Wang, Z. Gu, C. Duan, *Chem. Commun.* **2014**, *50*, 8651.
- [11] Y. P. Zong, X. H. Liu, X. W. Du, Y. R. Lu, M. Y. Wang, G. Y. Wang, *J. Environ. Sci. Health Part A* **2013**, *48*, 1583.
- [12] P. Kang, Z. Chen, S. O. Nielsen, K. Hoyt, S. D'Arcy, J. J. Gassensmith, Z. Qin, *Small* **2017**, *13*, 1.
- [13] D. A. Hastman, J. S. Melinger, G. L. Aragonés, P. D. Cunningham, M. Chiriboga, Z. J. Salvato, T. M. Salvato, C. W. Brown, D. Mathur, I. L. Medintz, E. Oh, S. A. Díaz, *ACS Nano* **2020**, *14*, 8570.
- [14] G. Zheng, S. de Marchi, V. López-Puente, K. Sentosun, L. Polavarapu, I. Pérez-Juste, E. H. Hill, S. Bals, L. M. Liz-Marzán, I. Pastoriza-Santos, J. Pérez-Juste, *Small* **2016**, 3935.
- [15] C. Carrillo-Carrión, R. Martínez, M. F. Navarro Poupard, B. Pelaz, E. Polo, A. Arenas-Vivo, A. Olgjati, P. Taboada, M. G. Soliman, Ú. Catalán, S. Fernández-Castillejo, R. Solá, W. J. Parak, P. Horcajada, R. A. Alvarez-Puebla, P. del Pino, *Angew. Chem. Int. Ed.* **2019**, *58*, 7078.
- [16] A. Wolf, L. Diestel, F. Lübckemann, T. Kodanek, T. Mohamed, J. Caro, D. Dorfs, *Chem. Mater.* **2016**, *28*, 7511.
- [17] A. Riedinger, P. Guardia, A. Curcio, M. A. García, R. Cingolani, L. Manna, T. Pellegrino, *Nano Lett.* **2013**, *13*, 2399.
- [18] R. R. Letfullin, C. Joenathan, T. F. George, V. P. Zharov, *Nanomedicine* **2006**, *1*, 473.
- [19] Y. Osaka, S. Sugano, S. Hashimoto, *Nanoscale* **2016**, *8*, 18187.
- [20] E. Lukianova-Hleb, Y. Hu, L. Latterini, L. Tarpani, S. Lee, R. A. Drezek, J. H. Hafner, D. O. Lapotko, *ACS Nano* **2010**, *4*, 2109.
- [21] W. M. Hanes, D. R. Lide, T. J. Bruno, *CRC handbook of chemistry and physics: a ready-reference book of chemical and physical data*, Vol. 95, **2014**.
- [22] H. Staleva, S. E. Skrabalak, C. R. Carey, T. Kosel, Y. Xia, G. V. Hartland, C. S. Kealley, M. B. Cortie, A. I. Maarroof, X. Wu, Y. Sun, M. Pelton, H. Wang, S. Zou, P. Chem, C. Phys, H. Okamoto, P. Chem, C. Phys, M. Rycenga, K. K. Hou, C. M. Cobley, G. Andrea, P. H. C. Camargo, Y. Xia, J. Rodríguez-fernández, A. M. Funston, R. A. Álvarez-puebla, L. M. Liz-marzán, P. Zijlstra, J. W. M. Chon, M. Gu, P. Chem, P. Zijlstra, J. W. M. Chon, M. Gu, *Phys. Chem. Chem. Phys.* **2009**, *11*, 5866.
- [23] S. Hashimoto, D. Werner, T. Uwada, *J. Photochem. Photobiol. C* **2012**, *13*, 28.
- [24] S. Inasawa, M. Sugiyama, Y. Yamaguchi, *J. Phys. Chem. B* **2005**, *109*, 3104.
- [25] D. Werner, S. Hashimoto, *J. Phys. Chem. C* **2011**, *115*, 5063.
- [26] N. M. Bulgakova, A. V. Bulgakov, *Appl. Phys. A Mater. Sci. Process.* **2001**, *73*, 199.
- [27] X. Zhang, J. Jiang, *J. Phys. Chem. C* **2013**, *117*, 18441.
- [28] H. D. Young, R. A. Freedman, *University Physics with Modern Physics in SI Units*, **2019**.
- [29] T. Tynell, A. Giri, J. Gaskins, P. E. Hopkins, P. Mele, K. Miyazaki, M. Karppinen, *J. Mater. Chem. A* **2014**, *2*, 12150.
- [30] X. Song, H. Sun, X. Cao, Z. Wang, D. Zhao, J. Sun, H. Zhang, X. Li, *RSC Adv.* **2016**, *6*, 112451.
- [31] A. Zanon, F. Verpoort, *Coord. Chem. Rev.* **2017**, *353*, 201.
- [32] M. N. Tahir, F. Natalio, M. A. Cambaz, M. Panthöfer, R. Branscheid, U. Kolb, W. Tremel, *Nanoscale* **2013**, *5*, 9944.
- [33] G. Lu, S. Li, Z. Guo, O. K. Farha, B. G. Hauser, X. Qi, Y. Wang, X. Wang, S. Han, X. Liu, J. S. Duchene, H. Zhang, Q. Zhang, X. Chen, J. Ma, S. C. J. Loo, W. D. Wei, Y. Yang, J. T. Hupp, F. Huo, *Nat. Chem.* **2012**, *4*, 310.
- [34] X. Liu, M. Atwater, J. Wang, Q. Huo, *Colloids Surf. B* **2007**, *58*, 3.
- [35] K. Momma, F. Izumi, *J. Appl. Crystallogr.* **2011**, *44*, 1272.
- [36] S. Graulis, D. Chateigner, R. T. Downs, A. F. T. Yokochi, M. Quirós, L. Lutterotti, E. Manakova, J. Butkus, P. Moeck, A. Le Bail, *J. Appl. Crystallogr.* **2009**, *42*, 726.

Manuscript received: April 12, 2022
Accepted manuscript online: April 25, 2022
Version of record online: May 5, 2022